



Full length article

Collagen fiber recruitment: A microstructural basis for the nonlinear response of the posterior pole of the eye to increases in intraocular pressure

Ning-Jiun Jan^{a,b}, Ian A. Sigal^{a,b,*}^a Department of Bioengineering, Swanson School of Engineering, University of Pittsburgh, Pittsburgh, PA, USA^b Department of Ophthalmology, University of Pittsburgh School of Medicine, University of Pittsburgh, Pittsburgh, PA, USA

ARTICLE INFO

Article history:

Received 10 November 2017
 Received in revised form 9 March 2018
 Accepted 14 March 2018
 Available online 21 March 2018

Keywords:

Optic nerve head
 Collagen crimp
 Lamina cribrosa
 Peripapillary sclera
 Intraocular pressure
 Recruitment
 Biomechanics

ABSTRACT

Our goal was to quantify and characterize how the collagen fiber crimp waviness of the lamina cribrosa (LC) and peripapillary sclera (PPS) changes with intraocular pressure (IOP). Thirteen sheep (ovine) eyes were immersion and perfusion fixed while maintaining IOP at 0, 10, 15, 20, or 50 mmHg. Coronal optic nerve head (ONH) sections (30 μ m) were imaged with polarized light microscopy (PLM) and analyzed for collagen fiber orientation and waviness (SD of fiber orientation). In the LC, the waviness of every LC beam was measured. In the PPS, at least 900 collagen bundles were measured per eye. Using the waviness at 50 mmHg IOP, we defined tissue-specific thresholds to determine the fraction of loaded or recruited fibers. We found that fiber waviness decreased with IOP ($P < 0.001$). At every IOP, the waviness of the collagen fibers, and the fraction of fibers recruited in the LC were smaller or equal than those of the PPS ($P < 0.001$). At 15 mmHg IOP, both LC and PPS had $\frac{3}{4}$ recruited fibers and $\frac{1}{4}$ left in reserve. The decreased waviness with IOP and associated fiber recruitment is experimental evidence of fiber-based nonlinear biomechanical behavior of the ONH. At all IOPs the PPS had an equal or larger fraction of fibers recruited than the LC. That both LC and PPS had the same fraction of recruited and reserve fibers at normal IOP suggests that this may be an optimal fraction of recruitment for healthy eyes. Whether this extends to human eyes remains unknown.

Statement of significance

Collagen fibers exhibit a natural waviness or crimp that largely determine the nonlinear biomechanics of soft tissue. Experimental measurements of crimp morphology in the sheep eye, and how it changes with intraocular pressure (IOP), however, are exceedingly sparse. We quantified how posterior eye crimp changes with increasing IOP. We found that the lamina cribrosa and peripapillary sclera have fundamentally different crimp, and with increasing IOP, have different proportions of fibers that straighten, or get recruited, versus remaining wavy, or in reserve. Interestingly, at physiologic IOP of 15 mmHg, both tissues had about $\frac{3}{4}$ fibers recruited and $\frac{1}{4}$ fibers in reserve, indicating there may be an optimal fraction of fibers.

© 2018 Acta Materialia Inc. Published by Elsevier Ltd. All rights reserved.

1. Introduction

Collagen is the main load-bearing component of the eye. The collagen fiber organization and hierarchical architecture play a central role in determining the mechanical behavior of soft tissues,

often more so than the chemical composition of the fibers [1–4]. Characterization of the collagen organization and architecture in the eye is therefore vital to understanding eye physiology, aging, and certain diseases, such as glaucoma. While substantial attention has been directed over the last two decades to characterizing ocular collagen anisotropy and the large scale nonlinear mechanical properties of ocular tissues, very little is known about the microstructural basis for the observed behavior. Thus, even though it is well established that the tissues of the eye are nonlinear at the macro scale, the underlying collagen characteristics that determine this nonlinearity remain unclear. At the microstructural level, it has been shown, by us [5,6] and others [7–10], that the collagen

* Corresponding author at: Ocular Biomechanics Laboratory, Department of Ophthalmology, University of Pittsburgh School of Medicine, 203 Lothrop Street, Eye and Ear Institute, Rm 930, Pittsburgh, PA 15213, USA.

E-mail addresses: ninj@OcularBiomechanics.com (N.-J. Jan), ian@OcularBiomechanics.com (I.A. Sigal).

URL: <http://www.OcularBiomechanics.com> (I.A. Sigal).

fibers of the eye exhibit natural undulations called crimp. Evidence in other tissues suggests that crimp is the basis for the nonlinear behavior observed at the macroscale, in a process of stretch-induced stiffening called fiber recruitment (Fig. 1). Based on this theory, Grytz and colleagues used inverse numerical models to predict ocular collagen crimp characteristics [11–13]. Their models, while powerful, involve major assumptions on the collagen crimp shape and recruitment with intraocular pressure (IOP), and their predictions have not been validated.

We recently demonstrated that polarized light microscopy (PLM) can be used to measure collagen fiber crimp characteristics of the lamina cribrosa (LC) and peripapillary sclera (PPS) [5]. The study, however, only considered IOPs below normal (0, 5 and 10 mmHg), and therefore did not provide information on normal or elevated IOPs. In addition, because the study focused on collagen crimp period, the information on stretch-induced uncrimping and recruitment was limited, compared with other parameters such as waviness [14,15]. To the best of our knowledge there are no other experimental measurements of collagen fiber crimp in the LC and PPS, or of the process of collagen fiber recruitment.

Our goal in this study was to quantify how ocular collagen crimp changes as IOP increases. Specifically, we quantify LC and PPS collagen crimp waviness at low, normal and elevated IOPs. An experimental characterization of the tissue recruitment at the microscale fiber-level is necessary to obtain a robust mechanistic understanding of how ocular tissues respond to loading in health and disease. Understanding uncrimping and recruitment is also useful to develop more accurate constitutive models to describe posterior pole tissue mechanics. Clinically, understanding how crimp morphology affects tissue mechanics and response to loads can augment our understanding of the biomechanical component of ocular diseases, including glaucoma. This could potentially impact diagnosis and treatment, for example through the detection or modification of sensitivity to IOP.

2. Methods

2.1. Specimen preparation

Thirteen eyes from two year old sheep were obtained from a local abattoir and processed within 24 h of death following the

process described elsewhere [5]. Briefly, the muscles, fat, and episcleral tissues were carefully removed using a combination of scalpels, razors, and forceps. Eyes were kept in $1\times$ phosphate buffered saline (PBS) with pH 7.4 until fixation. The eyes were cannulated through the anterior chamber and IOP set using a fluid column (Fig. 2). The eyes were immersion and perfusion fixed in 10% formalin for, at least, 12 h while maintaining IOP at 0, 10, 15, 20, or 50 mmHg, with at least one eye per pressure. Normal physiologic IOP in sheep is 10–15 mmHg [16]. Following fixation, the posterior poles were excised using a trephine 11.5 mm diameter and cryosectioned coronally into 30 μm thick slices. Due to the natural variability in the shape, position and orientation of the LC and PPS, as well as tilt during embedding and sectioning, some sections show better the LC or the PPS. To ensure robust analysis we made sure to have at least three good sections at the level of the LC and three good sections at the level of the PPS for each eye. Only sections free of artifacts, such as folds, were chosen.

2.2. Imaging

The sections were imaged using PLM following previously reported protocols [17]. Briefly, two polarized filters (Hoya, Tokyo, Japan) were used, one as polarizer placed before the sample, and the other as an analyzer placed after the sample. Four images were captured using white light illumination, with filter orientations rotated 45° between images. The relative changes in signal intensities at each pixel were used to compute local collagen fiber orientation. An Olympus SZX16 microscope was used with an Olympus DP80 camera (36-bit, RGB, pixel shift setting, Olympus, Tokyo, Japan), a $0.6\times$ reducer, and $0.8\times$ objective (numerical aperture 0.12). Images with 20% overlap were acquired using a manual stage, and stitched into mosaics using Fiji Is Just ImageJ (FIJI) [18].

To visualize the whole LC and scleral canal, 10–30 images were captured of each LC section using the $11.5\times$ magnification setting on the microscope ($0.37\ \mu\text{m}/\text{pixel}$). To visualize the PPS to the edge of the section, 20–40 images were acquired of the sections at the PPS level using the $4\times$ magnification setting on the microscope ($1.08\ \mu\text{m}/\text{pixel}$). In a previous study we demonstrated that the orientation information derived from PLM images are robust to changes in microscope-camera pairings and magnifications [17].

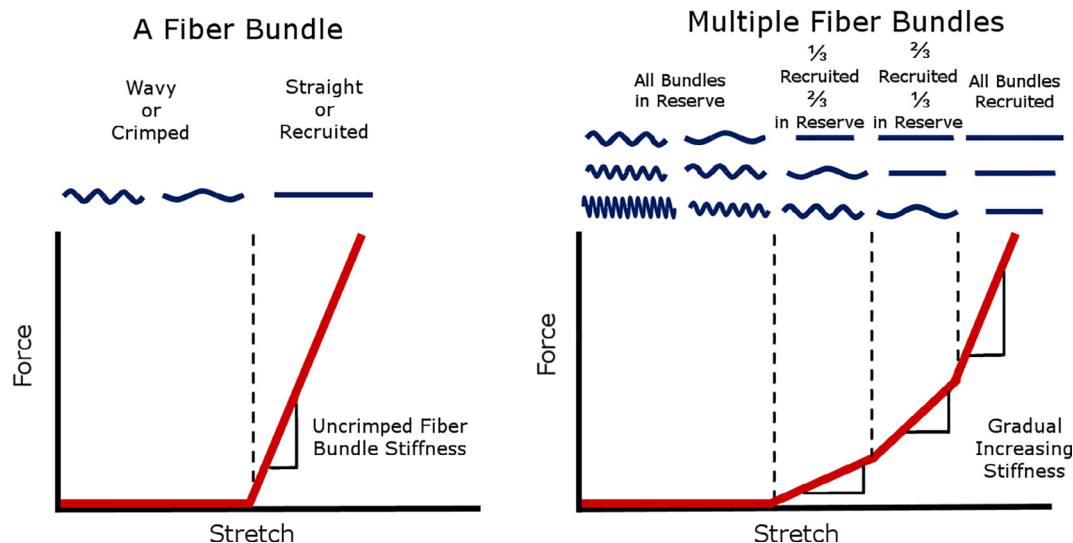


Fig. 1. Idealized plots of force vs stretch differ for a fiber bundle versus multiple fiber bundles. A fiber bundle is easy to stretch when it is crimped or wavy, however after the bundle is straight or recruited, the bundle becomes much stiffer, requiring more force to elongate the bundle. (Left) When many crimped fiber bundles with different amounts of slack are stretched together, the gradual straightening of the fibers creates a gradual, nonlinear stiffening, where more and more force is required to continue stretching the tissue. (Right) A fiber that is straightened is referred to as recruited. Conversely, a fiber that is not recruited, but would at higher stretch, is referred to as reserved. The proportion of fibers recruited to those in reserve is directly related to the rate of recruitment. Adapted from Jan et al. (2017) [5].

Experimental Setup

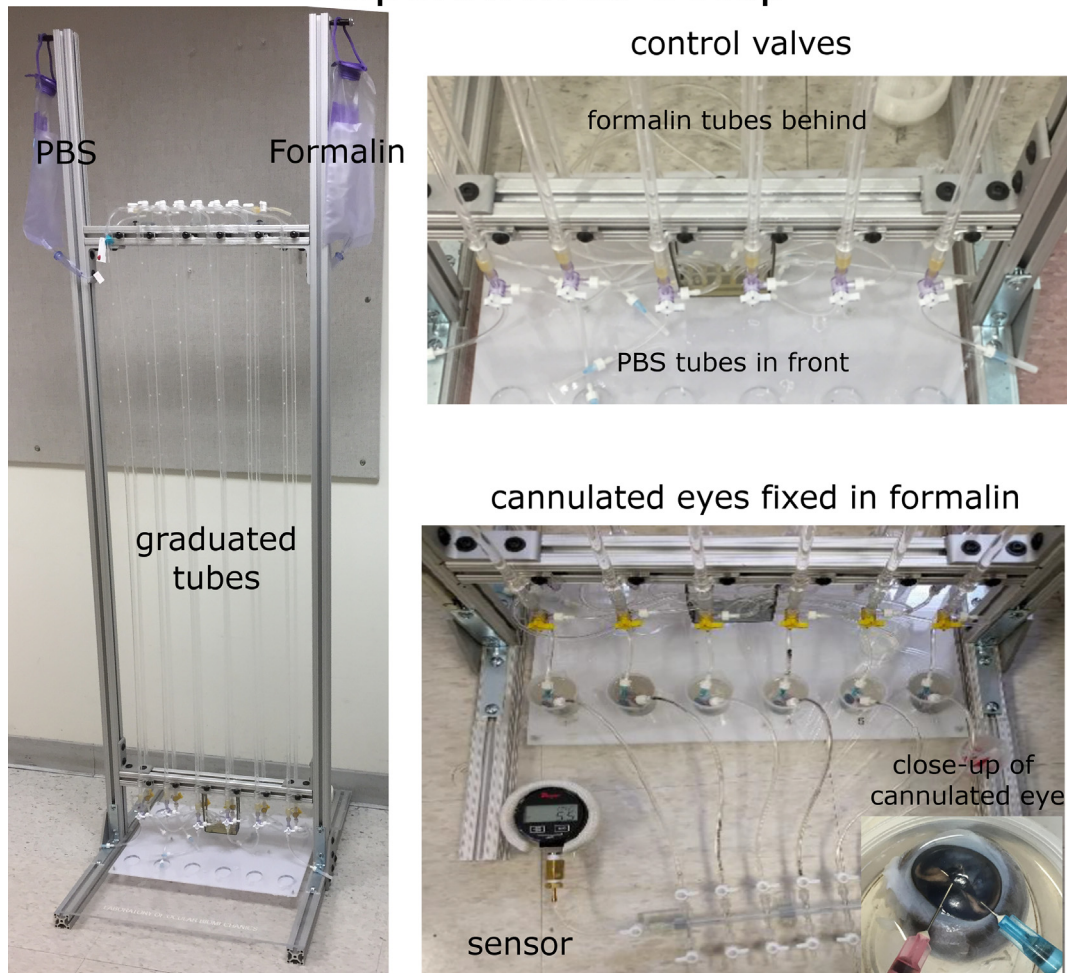


Fig. 2. Experimental setup for IOP control and globe fixation. IOP was set by controlling the height of a column of PBS from a reservoir. The system shown allows simultaneous processing of six eyes. Through the control valves we could switch the PBS to fixative, while maintaining IOP and flow. Eyes were double cannulated through the anterior chamber. Fixation is completed by also immersing the globes into fixative. The valve system also allows IOP monitoring through a sensor attached at the bottom right.

A lower magnification was used for the PPS to keep the number of images necessary similar to the LC.

2.3. Measuring collagen crimp recruitment

The collagen of the eye has a hierarchical structure, with fibrils forming fibers and fibers forming bundles. PLM is based on the optical properties of the collagen molecules, and therefore it allows accurate quantification of collagen orientation without the need to resolve and distinguish fibrils, fibers, or bundles. PLM orientation analysis is not dependent of identifying structure edges. In this work, we measured the spatial distribution of collagen molecule orientations along collagenous structures, and use these to determine waviness, and through the IOP-related changes of waviness the recruitment.

Using Fiji, straight lines were placed manually on the images along collagen bundles. When marking, attention was taken to do this only on bright clearly visible bundles. This helped ensure that the bundles were in the section plane, and minimize potential effects of out of plane orientation [19]. We were also careful to mark only LC beams and not the tree-like ventral groove or vessel walls. For each line, the PLM-derived collagen orientations of all the pixels along the line were compiled. As a measure of crimp, we computed the waviness for the line as the circular standard deviation of the

pixel angles. The wavier the fibers, the larger the spread of orientations, increasing the deviation and the waviness (Fig. 3). A useful property of this method to compute fiber waviness is that it is robust to the small deviations of measuring line orientation. The waviness was measured for every LC trabeculae beam and for, at least, 900 PPS collagen bundles per eye (Fig. 4). In preliminary tests, we noticed that even at very high IOP levels (above 50 mmHg), the collagen was not perfectly straight, with some residual waviness due to curved bundles or beams, and fiber interweaving. Quantifying this residual waviness was not our goal in this work. We were specifically focused on how the collagen crimp changes with IOP, rather than how curved or interwoven the bundles were. Therefore, based on the preliminary data observations, we defined tissue-specific waviness recruitment thresholds as the 90th percentile waviness in each tissue at 50 mmHg of IOP. If the waviness decreased below the tissue threshold, the collagen fiber bundle was considered recruited. To confirm that the results presented in this work are robust to the threshold chosen for recruitment, we varied the threshold for the PPS all the way down to 10th percentile.

2.4. Crimp visualization

Using previously reported methods, PLM images were further processed to enhance visualization of the collagen fiber crimp

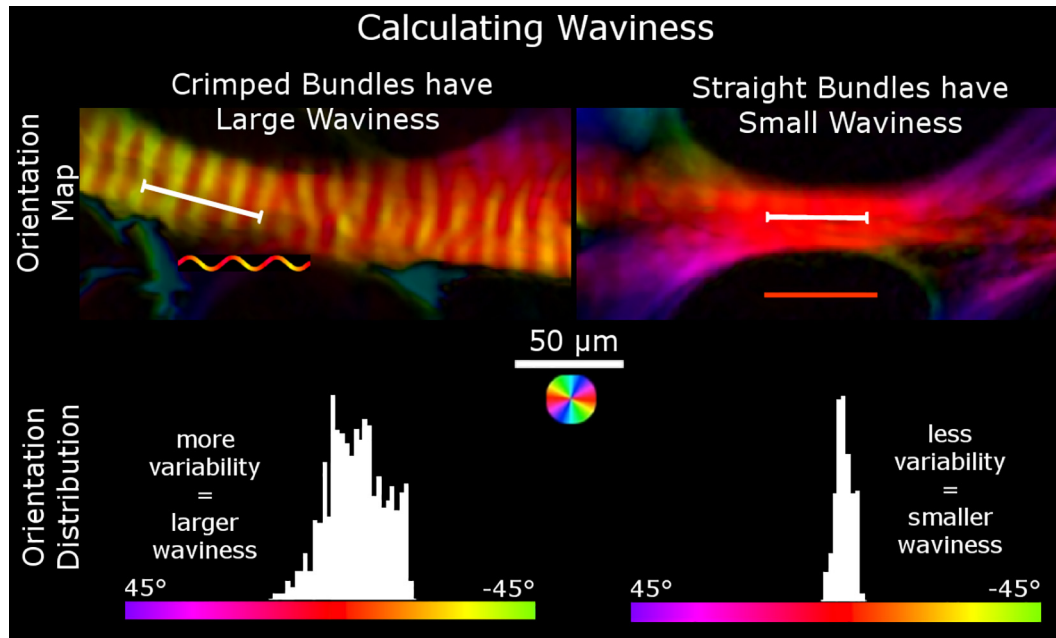


Fig. 3. Orientation maps of two trabeculae beams of the LC and the orientation distributions across lines (the white line segments) drawn along each beam. Waviness is calculated using the circular standard deviation of the collagen fiber orientations through a fiber bundle. The histograms show the distribution of orientations of the pixels under the line. In wavy crimped fiber bundles, the orientation distribution is more variable, resulting in larger waviness values (left) while in straight fibers, the distribution is less variable, resulting in smaller waviness values (right).

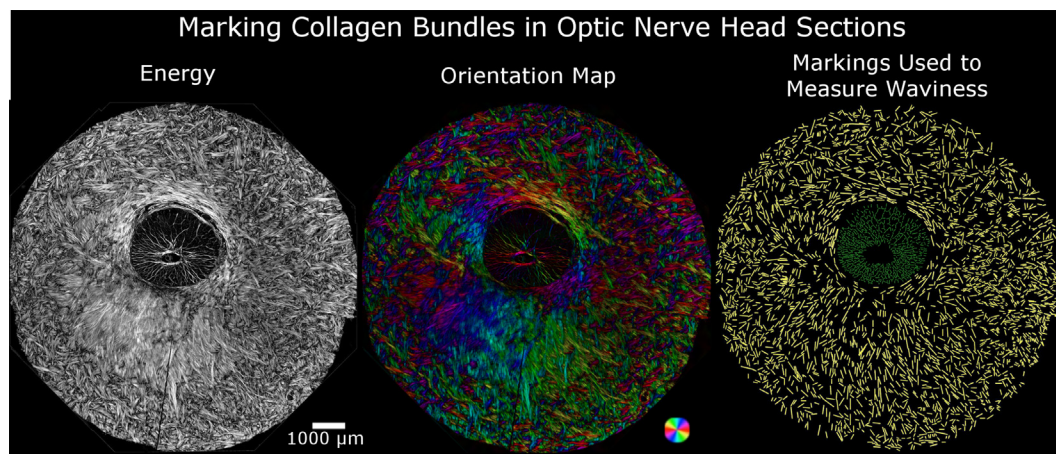


Fig. 4. Manual markings of collagen bundles in images of the ONH used to measure waviness. Example energy image of a coronal section of the posterior pole centered on the optic nerve head (left). Fiber distribution and orientation are best visualized using PLM-computed orientation with intensity scaled by energy (middle). Using manually placed lines, we measured the waviness in the PPS (yellow) and the LC (green). (For interpretation of the references to color in this figure legend, the reader is referred to the web version of this article.)

and their recruitment [5]. Briefly, the difference between each pixel's orientation and the average fiber orientation in its neighborhood (4 pixel radius, 1.5 µm for LC and 4.3 µm for the PPS) was calculated. The images were then pseudo-colored purple, if this difference was positive, or yellow if the difference was negative (Fig. 5). To aid visualization, pixel intensity was scaled by an “energy” parameter, previously described [17]. Briefly, energy measures the variations in pixel intensity with rotations of the polarized filters. Energy is zero if there is no change of intensity, such as outside of the tissue, and large when there is a substantial change in signal with angle. Scaling the images by energy simplifies discerning simultaneously the collagen crimp and tissue. A crimped, unrecruited fiber shows discernible bands of purple and yellow along the bundle. Uncrimped, recruited fibers do not have

discernible bands (Figs. 6 and 7). This visualization was especially useful for discerning the variability in orientation remaining at elevated IOP. (Fig. 7).

2.5. Statistical analysis

Linear mixed effect models accounting for correlations between measurements from the same sections, eyes, and animals were used to analyze how the waviness changed with pressure and the difference in waviness between the LC and PPS at each IOP. Descriptive statistical calculations such as angular mean and standard deviation were made using circular statistics [20]. All statistical analyses were done using R [21].

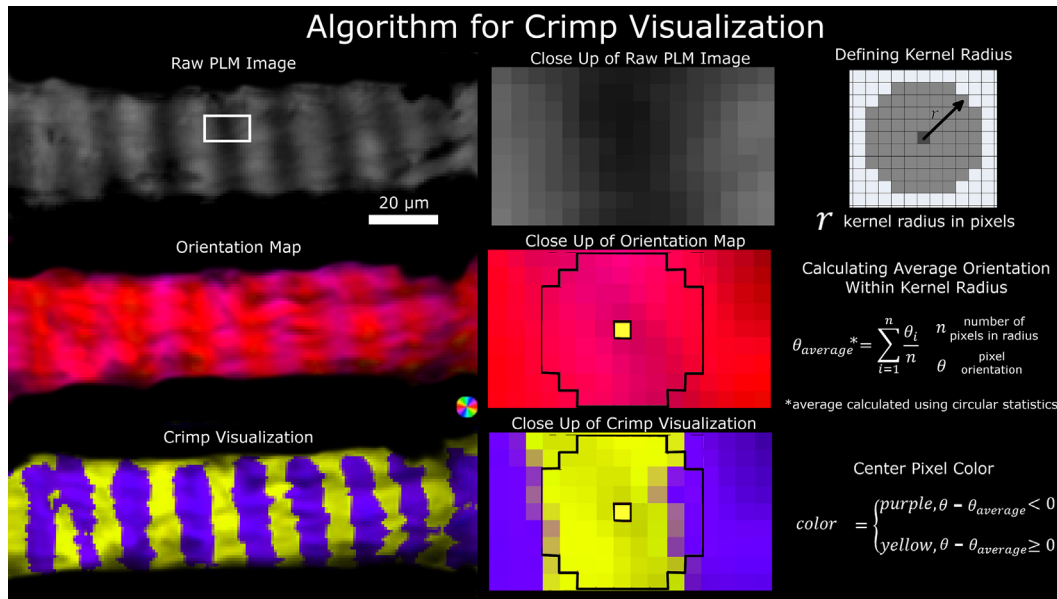


Fig. 5. Crimp visualization algorithm. A set of raw PLM images (top left) are used to calculate an orientation map (middle left). The orientations are further processed to simplify visualization of the crimp using yellow/purple bands (bottom left). The middle column shows close-ups of the LC beam region outlined in the white box in the top left panel. A kernel radius was defined (top right) and used to calculate the local average orientation (middle right). The center pixel was colored yellow or purple depending on the relative orientation of the pixel relative to the average orientation within the local kernel region (bottom right). A neighborhood of 4 pixels is shown in the close up of the orientation map and of the crimp visualization. The process is repeated for all pixels, then the pixel intensity scaled by the energy. (For interpretation of the references to color in this figure legend, the reader is referred to the web version of this article.)

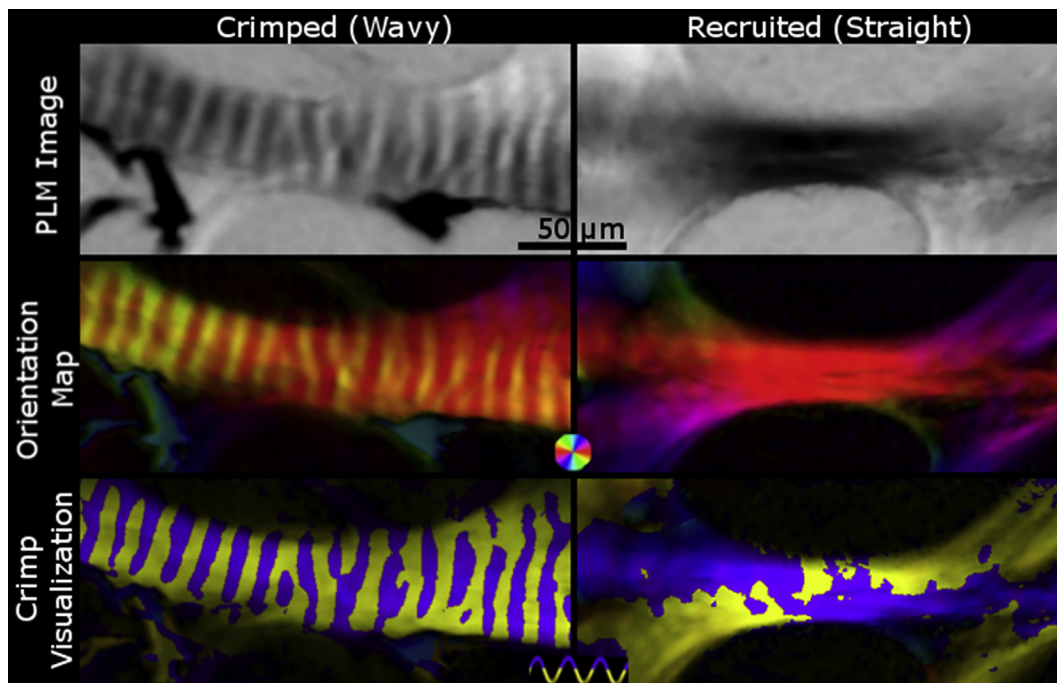


Fig. 6. The crimp visualization of a crimped fiber versus a straight fiber. Crimped, unrecruited wavy fibers (left) show changes in intensity in PLM images (top left), periodic changes in color in orientation maps (middle left), and distinct purple and yellow bands (bottom left). Recruited, straightened fibers (right), on the other hand, show a consistent intensity in PLM images (top right) and color in orientation maps (middle right), and patchy yellow and purple in the crimp visualization plot (bottom right). In addition, the crimp visualization of straight fibers fail to show clear bands of purple and yellow. (For interpretation of the references to color in this figure legend, the reader is referred to the web version of this article.)

3. Results

A total of 20,442 measurements of collagen crimp waviness were collected, of which 13,565 were of PPS collagen bundles and 6877 of LC beams across all eyes. From these measurements,

we quantified how the waviness of the fibers and percentage of fibers recruited in the LC and PPS changed with IOP (Fig. 8). We found that, while the exact fraction of fibers recruited varied with threshold percentile, the patterns and trends of recruitment did not change (Supplementary Material). The waviness' of the colla-

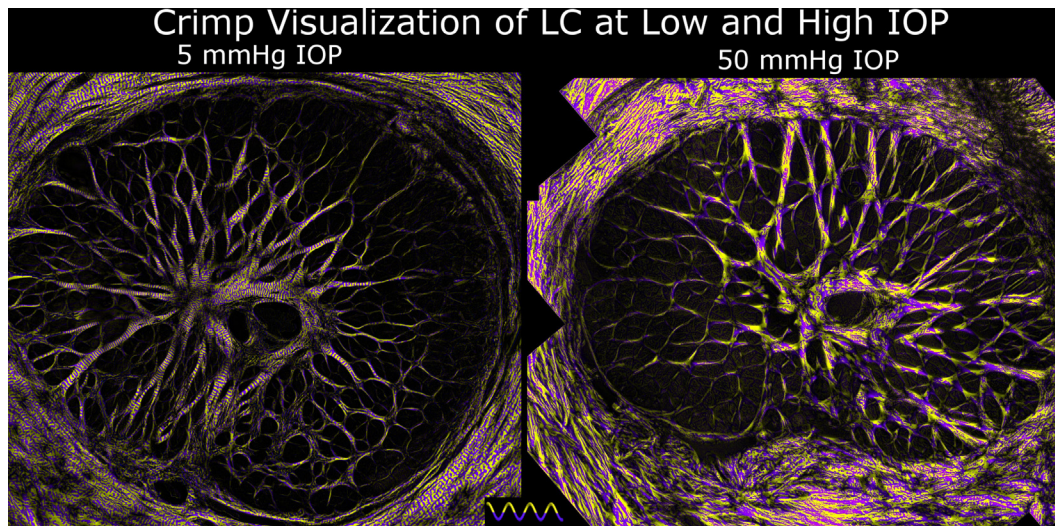


Fig. 7. Crimp in LC at low and elevated IOPs. Using the crimp visualization technique described in Fig. 5 evidences clear differences in crimp between LCs of eyes fixed at low (left) or elevated (right) IOPs. At 5 mmHg IOP, it is easy to distinguish across the whole LC periodic purple and yellow banding perpendicular to the LC trabeculae beams. In contrast, at 50 mmHg IOP, the LC beams show patchy or noisy yellow and purple coloring, indicative of recruited fibers. (For interpretation of the references to color in this figure legend, the reader is referred to the web version of this article.)

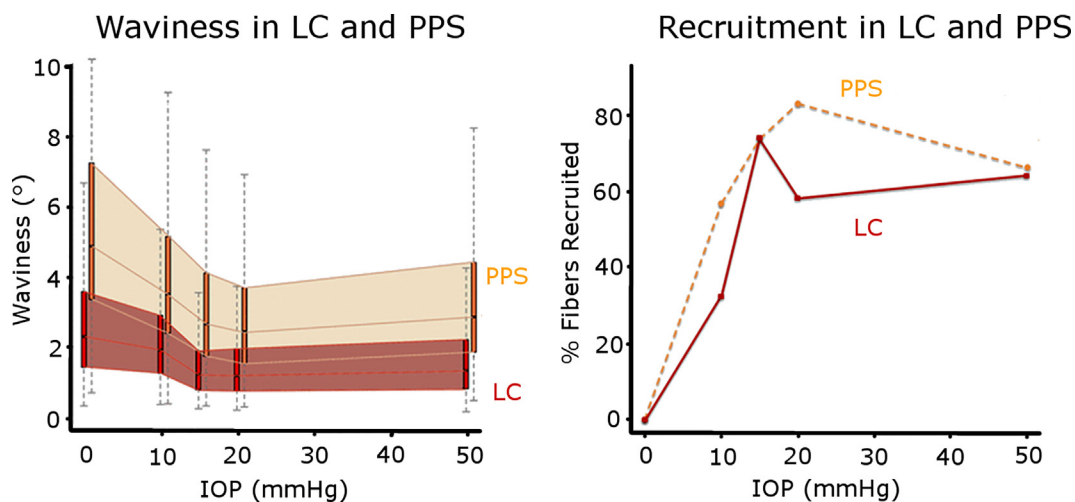


Fig. 8. Waviness and recruitment in the LC and PPS. At each IOP, we obtained the distributions of the collagen waviness in the LC (red) and PPS (orange), represented here as thin box plots. (left) The 25th to 75th percentiles of the waviness at each IOP were shaded to highlight the distinct differences between LC and PPS. The resulting recruitment curves were also significantly different between LC and PPS (right). The LC consistently had lower waviness than the PPS and also reserved the same or a larger percentage of fibers than the PPS at every IOP. At 15 mmHg both the LC and PPS had $\frac{3}{4}$ of their fibers recruited and $\frac{1}{4}$ in reserve. (For interpretation of the references to color in this figure legend, the reader is referred to the web version of this article.)

gen fibers in the LC and PPS were different, but had similar trends with increases in IOP. At every IOP, the LC fibers were less wavy than those in the PPS ($P < 0.001$) (Fig. 9). The fibers in the LC also had smaller standard deviation of their waviness compared to the fibers in the PPS at every IOP, indicating that waviness in the LC was more uniform than in the PPS. The waviness threshold above which a fiber was considered recruited was lower in the LC (3.4°) than in the PPS (6.7°), indicating that at baseline pressure the fibers in the LC are more straight than fibers in the PPS.

The recruitment curves for the LC and PPS were similar, but had important differences. Recruitment in both tissues was faster at lower IOPs (0–10, and 10–15 mmHg) than at higher IOPs (15–20, and 20–50 mmHg) ($P < 0.001$). At low IOPs more sclera fibers were recruited than LC fibers, such that at 10 mmHg about half of the sclera fibers had been recruited, compared with only a third in the LC. Between 10 and 15 mmHg, recruitment in the LC was faster

than in the PPS, such that, at 15 mmHg, $\frac{3}{4}$ of the fibers were recruited in both tissues, leaving a quarter of the fibers in reserve. Further increasing IOP to 20 mmHg caused an increase in PPS recruitment but a small decrease in the LC. These trends reversed for IOP increases between 20 mmHg and 50 mmHg as there was a slight increase in LC recruitment and a decrease in PPS recruitment.

4. Discussion

Our goal was to quantify the changes in LC and PPS collagen crimp waviness with IOP. Three main results arise from this work. First, the waviness of the collagen fibers decreased with increasing IOP. Second, at every IOP, the waviness of the collagen fibers in the LC was smaller and less variable than that of the PPS. Third, the LC

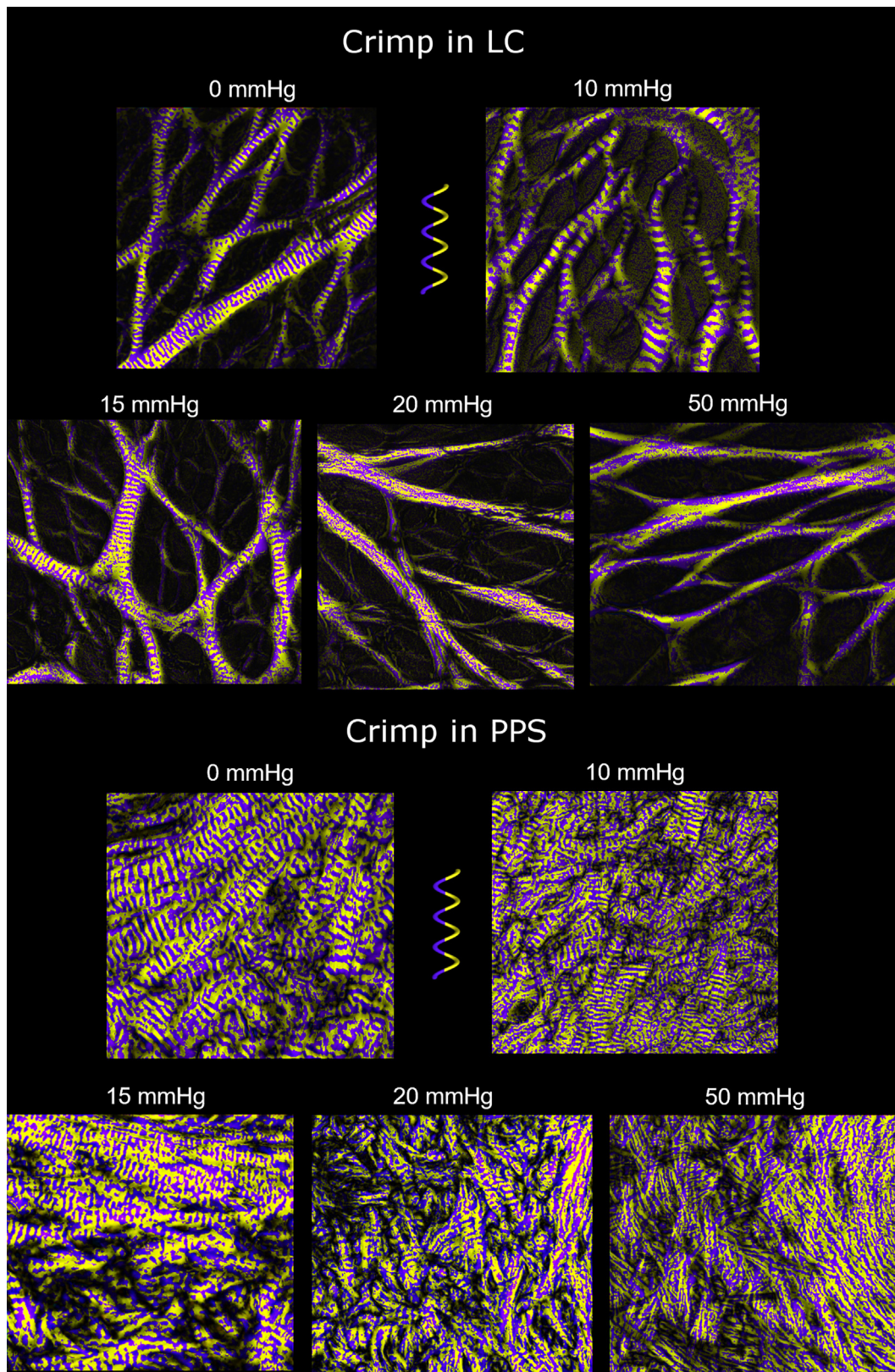


Fig. 9. Crimp visualizations of LC and PPS at various IOPs. The LC trabeculae beams gradually lose their crimp with increasing IOP. At 50 mmHg IOP, essentially all LC beams have been recruited. The PPS crimp gradually disappears with increasing IOP, though even at 20 mmHg IOP, some crimp is still apparent. Compared to the LC, the PPS had wavier fiber bundles at the same IOPs. The waviness in the LC and PPS was generally less than 10°. Midgett et al. (2017) reported strains below 3% even at IOPs of 45 mmHg which agrees with the small waviness we found for the LC [26]. For reference, in unpublished studies of sheep Achilles' tendon, we found the average waviness to be greater than 20°, which agrees with the large extensibility of tendon fibers.

and PPS have different recruitment curves. Let us consider each of these in turn:

The waviness of the collagen fibers decreased with increasing IOP. The decreasing waviness with increasing IOP is consistent with current theory of collagen fiber recruitment in soft tissues, in which the fibers straighten with stretch to become recruited, contributing to the local stiffening of the tissue. While this phenomenon is well recognized in other tissues, like tendon and ligament [22–24], this study is the first experimental evidence in the posterior pole.

At every IOP, the waviness of the collagen fibers in the LC was smaller and less variable than that of the PPS. These differences in crimp morphology suggest that there are also distinct differences between the LC and PPS biomechanical properties. In other tissues the variability of the crimp morphology is a major determinant of how gradually the tissue stiffens under tensile load. In tissues with uniform crimp morphology, fibers require the same amount of stretch to straighten, resulting in a step recruitment and a consequent sudden stiffening. Alternatively, in tissues with variable crimp morphology, fibers require different amounts of stretch to straighten, resulting in a gradual recruitment and stiffening. We have shown that the fibers of the LC have a somewhat uniform waviness at low IOPs, and a marked decrease in waviness between 10 and 15 mmHg. The fibers of the PPS, in contrast, had more waviness at low IOPs and a more gradual decrease in waviness from 0 to 20 mmHg. These results suggest that the LC stiffens abruptly between 10 and 15 mmHg, whereas the PPS gradually stiffens from 0 to 20 mmHg IOP. Experimental studies of ex-vivo inflation have not reported a steep change in strain with increasing IOP [25,26]. They observed a relatively smooth decrease in the IOP-induced strains with IOP increases, consistent with the recruitment reported in this work. Some of the differences could be due to different IOP levels studied, or could be inter-species differences. Most importantly, the relationships between strain, stiffness, recruitment, and IOP are complex, making it difficult to make a direct quantitative comparison beyond the general trends of increasing stiffness with IOP. Future studies could correlate strain with changes in crimp and recruitment to elucidate the complexities of ONH mechanics.

It is important to note that the uncrimping or recruitment only relates to the rate of stiffening with IOP, which may be very different from overall tissue stiffness. The results above should, therefore, not be interpreted to mean that the LC is stiffer than the sclera. This study provides data that helps explain how the complex nonlinear properties of the LC and PPS arise from the collagen fibers microarchitecture and morphology. In addition to fiber uncrimping, other factors may affect overall tissue biomechanics, such as fiber reorientation and the biomechanical properties of the fibers themselves after straightening. Elsewhere, studies of collagen suggest that straight collagen fibers have a response to stretch that is close to linear up to the point of damage [1]. We did not observe any clear fiber reorientations with IOP in the tissues of the posterior pole are small, but a systematic study is needed to fully account for these effects on the tissue properties.

The LC and PPS have different recruitment curves. At every IOP an equal or larger percentage of the PPS fibers was recruited than LC fibers. Because recruited fibers are the fibers that bear load, our results reveal interesting information on the relative fraction of potentially load-bearing fibers of each tissue that are bearing load. At 10 mmHg, a low, but still physiologic IOP, twice as much of the PPS (~60%) than of LC (~30%) participated in bearing loads. Interestingly, at physiologic IOP of 15 mmHg, the same fraction (~3/4) of LC and PPS fibers was recruited, keeping ¼ of their fibers uncrimped as a reserve. This 3 to 1 ratio of loaded vs. reserved fibers at physiologic IOP for both LC and PPS, may indicate a target ratio where fibers of the LC and PPS have remodeled their crimp

morphology for optimal function in their typical biomechanical environment. At IOP of 20 mmHg, at the upper edge of the normal pressure range, we found that the PPS recruited more fibers whereas the LC recruited less. This may be a protective mechanism, whereby the PPS bears more load in order to relieve the LC and protect the retinal ganglion cell axons. It is also possible that the decrease is due to differences between eyes. Studies in other tissues like arterial walls have shown similar unexplained trends where the percentage of recruited fibers drops at high strains [27]. Further studies are needed to understand the decrease in percentage of fibers recruited in the LC from 20 to 25 mmHg and in the PPS from 20 to 50 mmHg.

The importance of collagen fiber crimp and recruitment in soft tissue mechanics has been recognized for over 40 years by several groups. The majority of studies have analyzed how crimp morphology changes with mechanical stimuli in tendon and ligament. In 1972, Diamant and colleagues quantified the crimp angle and period in tendon, and how much stretch was required to make a fiber bundle straight, or recruited [28]. More recently, Hansen and colleagues quantified the collagen crimp period in tendon under stretch while imaging using optical coherence tomography [23]. For ligaments, Thornton and colleagues used PLM and scanning electron microscopy to calculate the percentage of crimped area stretched in situ under different amounts of stress [24]. The crimp period and angle were measured for a few fibers in each area and the percentage of uncrimped area was used to track the collagen crimp recruitment. Besides tendon and ligament, recruitment curves have also recently been experimentally derived for arterial tissue and used in microstructural fiber-based models to predict tissue responses [27,29,30]. For example, a study by Hill and colleagues measured the collagen crimp tortuosity, the ratio between a fiber's arc length to its chord length using manual fiber tracings of multiphoton images [27]. A collagen fiber was considered recruited if the tortuosity of a fiber dropped below a certain threshold. Manual measurements were used to fit a recruitment curve.

The importance of crimp and recruitment has likewise been noted in the ocular biomechanics community, though there is a significant lack of experimental data on collagen fiber crimp and recruitment in the eye compared to other tissues. Grytz and colleagues predicted the collagen crimp microstructure in the corneal shell using stress-strain curves gathered from mechanical tests and a constitutive model that assumed that all collagen fibers within a tissue (i.e. cornea or sclera) had uniform helical spring morphology [11,12]. In this model the shape of the stress-strain curve could be determined by just the crimp angle and the amplitude of the crimp relative to the fiber thickness. The crimp angle determined the inflection point in the stress-strain curve, while the amplitude relative to fiber thickness determined the nonlinearity of the curve. The model by Grytz and colleagues considered the nonlinearity of the stress-strain curve as arising from fiber uncrimping, rather than recruitment. These are related, but not the same. We have found direct experimental evidence that the crimp morphology in the LC and PPS is highly inhomogeneous, and that both tissues gradually recruit their collagen fibers with increasing IOP-induced stretch. Using inverse modeling of the posterior pole Grytz and colleagues postulated that age-related stiffening in the eye is due to a changing ground matrix, though this has not been verified experimentally [31]. The connection between tissue stiffness and aging, and age-related diseases underscores the importance of identifying the fundamental basis for changes in tissue stiffness, and the need for experimental validation of theoretical predictions.

We recently quantified collagen crimp period and its spatial distribution in the LC and PPS at low IOPs [5]. Consistent with this work, we found that crimp periods in the PPS were larger than in the LC. In addition, in the PPS the period increased with distance

from the canal, whereas within the LC the period did not vary significantly. Liu and colleagues quantified crimp in the cornea using transmitted electron microscopy (TEM), measuring the angle of fibers in strips of cornea stretched uniaxially [32]. Others have visualized the crimp in the eye using electron micrographs [7], second harmonic generated (SHG) imaging [33], and magnetic resonance imaging (MRI) [10]. These studies, however, did not quantify any crimp morphology.

Studies of collagen fiber architecture of the posterior pole have typically focused on the organization at a scale larger than crimp [6]. For example, for the LC, trabeculae beam and pore diameters have been described using electron microscopy [34], histology [35], second harmonic generated imaging (SHG) [36], and optical coherence tomography (OCT) [37]. The sclera macro-scale anisotropy has been quantified using small angle light scattering (SALS) [38] and wide-angle X-ray scattering (WAXS) [39–41] for the collagen orientation, and polarization sensitive OCT (PS-OCT) for collagen birefringence [42]. Accurate measurement of micrometer-scale crimp properties, however, requires high angular and spatial resolutions, otherwise the orientation information will encode both anisotropy and crimp [43]. In addition, representative characterization over the LC and PPS requires a wide field of view, and comparability between tissues requires a sensitivity range spanning the low density of the LC and the high density of the PPS. It is possible to quantify crimp using other modalities. For example, SHG has excellent specificity for collagen and can image areas with micrometer-scale resolution. However, SHG protocols are more complex and the system itself is substantially more expensive. Most current methods of analyzing SHG images require resolving collagen fiber edges for tracing or for gradient-based analysis [27,29]. In areas of the ONH that have densely packed collagen with complex overlapping structures, it becomes much more difficult to ensure there are no artifacts. This is particularly difficult in areas with pigment [44], where the power of the SHG laser also increases the likelihood of thermal damage on the tissue. We have demonstrated that our implementation of PLM does not have these limitations and is suitable for characterizing ocular collagen crimp, even in densely packed areas with overlapping collagen fiber bundles [17].

In addition, sample preparation for PLM analysis of crimp is relatively simple as the tissues can be visualized without the need for dehydration, labels or stains, reducing tissue processing and the likelihood of introducing artifacts, such as deformation. Dehydration, necessary for paraffin and plastic embedding, and for most block-face imaging, causes substantial shrinkage of the tissues. Tissue flattening via stress-relieving cuts, such as those used in some studies with SALS or WAXS [38,39] could affect the collagen crimp. These were not necessary for PLM of cryosections.

It is important to consider the limitations of our study together with its strengths. The tissues used in this study were ex-vivo, fixed in formalin, and cryosectioned, each of which could introduce artifacts. In preliminary tests we tested fixing the eyes for 24 h, and longer, and did not detect any differences. Nevertheless, it is still possible that the tissues were not perfectly fixed by 12 h of formalin. If so, some crimp could “reappear” when the fixation pressure is removed, increasing the waviness observed at elevated IOP. We have previously shown that the tissue processing steps have minimal effects on tissue size and shape [45]. The study was conducted on sheep eyes from an abattoir. This is advantageous for a first study of this type, as animals bred together for human consumption may exhibit less inter-individual variations than human donors would. Sheep eyes have a collagenous LC, but also have distinct structural differences from humans, potentially limiting the application of our findings. Sheep LC have a thick tree-like ventral groove in the ONH, which humans do not have and it is possible that the crimp patterns we have found using sheep may not be applicable to humans. In this work we analyzed only LC beams.

Though understanding sheep as an animal model is important, measurements of crimp in other animals and humans are needed to understand how their microstructural crimp changes with IOP.

Another limitation of our study was that we tracked changes in collagen crimp using different samples for each IOP rather than measuring the crimp in the same sample through different IOPs. It is more akin to a cross-sectional than to a longitudinal study. It is possible that the variability between eyes may influence the recruitment trends observed. Future studies are necessary to confirm these trends, for example by using PLM to image fresh tissue at various levels of stretch, tracking individual fibers in situ [46,47] or using SHG [26,48].

Our measures of crimp waviness are based on the in-plane collagen fiber orientation derived from 2D histological sections of the ONH. The fiber orientation information can be biased depending on the direction of sectioning. However, we section the ONH coronally, which is the direction the ONH tissue experiences the majority of the IOP-induced forces. Our measurements of collagen crimp in the coronal plane would therefore be most relevant to the biomechanics of the eye. To limit our study to the in-plane fiber bundles from our coronal sections, we were careful to mark only in locations with bright well-defined bundles that appear in the section plane. In the LC, there are beams that can run oblique or even perpendicular to our plane of sectioning. These bundles would not be bright nor would they be well defined in our coronal PLM images, and therefore would not be included in the analyses. Future studies, should quantify the crimp changes with IOP in the sagittal and axial planes. Alternatively, it may be possible to do a full 3D analysis of crimp from coronal sections using more advanced PLM analysis methods [19].

As mentioned previously, the waviness of the LC and PPS fibers from eyes fixed at 50 mmHg IOP was used to determine the threshold for recruitment. We assumed that at the very high pressure of 50 mmHg, the vast majority of the fibers have been recruited, so any remaining waviness was not due to the collagen crimp. By using a threshold less than the 100% percentile, this allowed us to avoid considering beam or bundle curvature and interweaving as waviness. We recognize that there is some degree of arbitrariness in choosing the threshold percentile. Hence, we repeated the recruitment analyses using a wide range of threshold percentiles. We found that, although the percentage of fibers recruited changed with the threshold, the recruitment patterns for the LC and PPS were very similar (Supplementary Material). Hence, we conclude that our choice of threshold was not a determinant of the result.

We analyzed the percentage of fibers recruited for eyes fixed at 0, 10, 15, 20, and 50 mmHg IOP. The pressures were carefully chosen so that we could analyze the collagen crimp morphology in the no-IOP, physiologic, slightly higher pressure than physiologic, and extremely high pressure states. The lowest and highest pressure states were used to quantify the crimp at its waviest and least wavy. The three pressures in the middle were used to quantify the crimp at the states we suspected most of the recruitment would happen, which would be the transition from physiologic pressure through slightly higher pressures. This set of pressures provides a general shape of the recruitment curve. A more detailed characterization of the recruitment curve would require more pressures.

Collagen crimp waviness is but one parameter of the crimp morphology. There are other crimp characteristics that may also be important in determining how the crimp changes with stretch. For example, the amplitude, tortuosity, period, and maximum deviation angle can also be used to describe the crimp. In a previous study, we quantified the collagen crimp period in the posterior pole at low IOPs [5]. Grytz and colleagues predicted the maximum deviation angle using inverse modeling [12], while Robertson and

colleagues manually measured the tortuosity of the collagen fibers from SHG images [27]. Each of these parameters may potentially have different relationships with stretch. In addition, several other factors also affect tissue stiffness and response to load, including, but not limited to, fiber reorientation, fiber slip, tissue composition, collagen type, proteoglycan content and distribution and the amount and type of cross-linking between the fibers [1,22,49,50]. Therefore, studies considering additional tissue characteristics are needed to fully characterize the tissue response to load. In this study we did not split the LC or PPS into regions. This may be important and necessary to detect potential region-dependent variations, which may be of importance for sensitivity to IOP or susceptibility to disease [51].

An important goal of this work was to provide experimental measures of crimp morphology to help drive fiber-based constitutive model formulations for the posterior pole [13,52–54]. Although we obtained recruitment curves with IOP, we did not measure the stresses and strains within the LC and PPS. Our results will have to be integrated with other studies to derive the constitutive models.

In conclusion, we quantified the collagen crimp waviness in the LC and PPS at a wide range of IOPs. We derived tissue-specific recruitment curves and found that the LC and PPS have distinct crimp distributions and recruitment behaviors. Our results suggest that at a normal 15 mmHg of IOP, both the LC and PPS have about ¾ of the collagen recruited or “bearing load” and about ¼ crimped or “in reserve” to bear loads and increase stiffness at higher IOPs. The recruitment curves also suggest that there may be a protective mechanism whereby the PPS relieves some tension from the LC and reduce the fraction of loaded fibers at elevated IOPs. Altogether, our findings have demonstrated a strong link between the microstructural collagen crimp properties of the LC and PPS and IOP.

Proprietary interest

None.

Funding

This work was supported by the National Institutes of Health R01-EY023966, R01-EY025011, P30-EY008098.

Acknowledgements

We would like to acknowledge the people that helped make measurements for this study: Saundria Moed, James Constantin, Michael Iasella, Sarah Smelko, Ryan O'Malley, Natalie Rutkowski, and Michael Ulrich. This work was supported by National Institutes of Health R01-EY023966 and P30-EY008098.

Appendix A. Supplementary data

Supplementary data associated with this article can be found, in the online version, at <https://doi.org/10.1016/j.actbio.2018.03.026>.

References

- [1] P. Fratzl, *Collagen: Structure and Mechanics*, Springer Science & Business Media, New York City, NY, 2008.
- [2] S.A. Wainwright, W. Biggs, J. Currey, J. Gosline, *Mechanical Design in Organisms*, Princeton University Press, Princeton, NJ, 1982.
- [3] K.J. Niklas, *Plant Biomechanics: An Engineering Approach to Plant Form and Function*, University of Chicago Press, Chicago and London, 1992.
- [4] C. Mattheck, *Design in Nature: Learning from Trees*, 1st ed., Springer-Verlag Berlin Heidelberg, Berlin Heidelberg, 1998.

- [5] N.-J. Jan, C. Gomez, S. Moed, A.P. Voorhees, J.S. Schuman, R.A. Bilonick, I.A. Sigal, Microstructural crimp of the lamina cribrosa and peripapillary sclera collagen fibers, *Invest. Ophthalmol. Vis. Sci.* 58 (9) (2017) 3378–3388.
- [6] N.-J. Jan, K. Lathrop, I.A. Sigal, Collagen architecture of the posterior pole: high-resolution wide field of view visualization and analysis using polarized light microscopy, *Invest. Ophthalmol. Vis. Sci.* 58 (2) (2017) 735–744.
- [7] R. Andreo, R. Farrell, Corneal small-angle light-scattering theory: wavy fibril models, *J. Opt. Soc. Am.* 72 (11) (1982) 1479–1492.
- [8] K.M. Meek, N.J. Fullwood, Corneal and scleral collagens – a microscopist's perspective, *Micron* 32 (3) (2001) 261–272.
- [9] M. Winkler, G. Shoa, Y. Xie, S.J. Petsche, P.M. Pinsky, T. Juhasz, D.J. Brown, J.V. Jester, Three-dimensional distribution of transverse collagen fibers in the anterior human corneal stroma, *Invest. Ophthalmol. Vis. Sci.* 54 (12) (2013) 7293–7301.
- [10] L.C. Ho, I.A. Sigal, N.-J. Jan, A. Squires, Z. Tse, E.X. Wu, S.-G. Kim, J.S. Schuman, K. C. Chan, Magic angle-enhanced MRI of fibrous microstructures in sclera and cornea with and without intraocular pressure loading, *Invest. Ophthalmol. Vis. Sci.* 55 (9) (2014) 5662–5672.
- [11] R. Grytz, G. Meschke, Constitutive modeling of crimped collagen fibrils in soft tissues, *J. Mech. Behav. Biomed. Mater.* 2 (5) (2009) 522–533.
- [12] R. Grytz, G. Meschke, A computational remodeling approach to predict the physiological architecture of the collagen fibril network in corneo-scleral shells, *Biomech. Model. Mechanobiol.* 9 (2) (2010) 225–235.
- [13] R. Grytz, G. Meschke, J.B. Jonas, The collagen fibril architecture in the lamina cribrosa and peripapillary sclera predicted by a computational remodeling approach, *Biomech. Model. Mechanobiol.* 10 (3) (2011) 371–382.
- [14] I.A. Sigal, J.L. Grimm, N.-J. Jan, R.A. Bilonick, G. Wollstein, L. Kagemann, H. Ishikawa, J.S. Schuman, K. Davoli, K.L. Lathrop, IOP elevation reduces the waviness of the load bearing collagen fibers in the lamina cribrosa, *Invest. Ophthalmol. Vis. Sci.* 54 (15) (2013) 3158–3158.
- [15] I.A. Sigal, N.-J. Jan, S. Moed, R. O'Malley, H. Tran, R.A. Bilonick, H. Ishikawa, L. Kagemann, J.S. Schuman, G. Wollstein, A microstructural basis for nonlinear effects of IOP on the lamina cribrosa and sclera, *Invest. Ophthalmol. Vis. Sci.* 56 (7) (2015) 4821–4821.
- [16] M.S. Ghaffari, M. Shojaei, A. Sabzevari, N. Khorami, Reference values for intraocular pressure and Schirmer tear test in clinically normal Sanjabi sheep, *Small Rumin. Res.* 97 (1–3) (2011) 101–103.
- [17] N.-J. Jan, J.L. Grimm, H. Tran, K.L. Lathrop, G. Wollstein, R.A. Bilonick, H. Ishikawa, L. Kagemann, J.S. Schuman, I.A. Sigal, Polarization microscopy for characterizing fiber orientation of ocular tissues, *Biomed. Opt. Express* 6 (12) (2015) 4705–4718.
- [18] S. Preibisch, S. Saalfeld, P. Tomancak, Globally optimal stitching of tiled 3D microscopic image acquisitions, *Bioinformatics* 25 (11) (2009) 1463–1465.
- [19] B. Yang, N.-J. Jan, P. Lam, K.L. Lathrop, I.A. Sigal, Collagen architecture in the third dimension: 3D polarized light microscopy (3DPLM) for mapping in-plane (IP) and out-of-plane (OOP) collagen fiber architecture, *Invest. Ophthalmol. Vis. Sci.* 58 (8) (2017) 4825–4825.
- [20] S.R. Jammalamadaka, A. Sengupta, *Topics in Circular Statistics*, World Scientific Publishing Co., 2001.
- [21] R.C. Team, *R Foundation for Statistical Computing*, vol. 3, Vienna, Austria, 2013.
- [22] G.A. Holzapfel, *Handbook of Materials Behavior Models*, Academic Press, San Diego, CA, 2001.
- [23] K.A. Hansen, J.A. Weiss, J.K. Barton, Recruitment of tendon crimp with applied tensile strain, *J. Biomech. Eng.* 124 (1) (2001) 72–77.
- [24] G.M. Thornton, N.G. Shrive, C.B. Frank, Ligament creep recruits fibres at low stresses and can lead to modulus-reducing fibre damage at higher creep stresses: a study in rabbit medial collateral ligament model, *J. Orthop. Res.* 20 (5) (2002) 967–974.
- [25] B. Coudrillier, D.M. Galdes, N.T. Vo, R. Atwood, C. Reinhard, I.C. Campbell, Y. Raji, J. Albon, R.L. Abel, C.R. Ethier, Phase-contrast micro-computed tomography measurements of the intraocular pressure-induced deformation of the porcine lamina cribrosa, *IEEE Trans. Med. Imaging* 35 (4) (2016) 988–999.
- [26] D.E. Midgett, M.E. Pease, J.L. Jefferys, M. Patel, C. Franck, H.A. Quigley, T.D. Nguyen, The pressure-induced deformation response of the human lamina cribrosa: analysis of regional variations, *Acta Biomater.* 53 (2017) 123–139.
- [27] M.R. Hill, X. Duan, G.A. Gibson, S. Watkins, A.M. Robertson, A theoretical and non-destructive experimental approach for direct inclusion of measured collagen orientation and recruitment into mechanical models of the artery wall, *J. Biomech.* 45 (5) (2012) 762–771.
- [28] J. Diamant, A. Keller, E. Baer, M. Litt, R. Arridge, Collagen; ultrastructure and its relation to mechanical properties as a function of ageing, *Proc. R. Soc. Lond. B: Biol. Sci.* 180 (1060) (1972) 293–315.
- [29] B. Fata, C.A. Carruthers, G. Gibson, S.C. Watkins, D. Gottlieb, J.E. Mayer, M.S. Sacks, Regional structural and biomechanical alterations of the ovine main pulmonary artery during postnatal growth, *J. Biomech. Eng.* 135 (2) (2013) 0210221–0210221.
- [30] B. Fata, W. Zhang, R. Amiri, M.S. Sacks, Insights into regional adaptations in the growing pulmonary artery using a meso-scale structural model: effects of ascending aorta impingement, *J. Biomech. Eng.* 136 (2) (2014) 0210091–0210091.
- [31] M.A. Fazio, R. Grytz, J.S. Morris, L. Bruno, S.K. Gardiner, C.A. Girkin, J.C. Downs, Age-related changes in human peripapillary scleral strain, *Biomech. Model. Mechanobiol.* 13 (3) (2014) 551–563.

- [32] X. Liu, L. Wang, J. Ji, W. Yao, W. Wei, J. Fan, S. Joshi, D. Li, Y. Fan, A mechanical model of the cornea considering the crimping morphology of collagen fibrils, *Invest. Ophthalmol. Vis. Sci.* 55 (4) (2014) 2739–2746.
- [33] M. Winkler, D. Chai, S. Kriling, C.J. Nien, D.J. Brown, B. Jester, T. Juhász, J.V. Jester, Nonlinear optical macroscopic assessment of 3-D corneal collagen organization and axial biomechanics, *Invest. Ophthalmol. Vis. Sci.* 52 (12) (2011) 8818–8827.
- [34] A. Thale, B. Tillmann, The collagen architecture of the sclera—SEM and immunohistochemical studies, *Ann. Anat.* 175 (3) (1993) 215–220.
- [35] M.R. Hernandez, X.X. Luo, F. Igoe, A.H. Neufeld, Extracellular matrix of the human lamina cribrosa, *Am. J. Ophthalmol.* 104 (6) (1987) 567–576.
- [36] I.A. Sigal, J.G. Flanagan, I. Tertinegg, C.R. Ethier, Finite element modeling of optic nerve head biomechanics, *Invest. Ophthalmol. Vis. Sci.* 45 (12) (2004) 4378–4387.
- [37] B. Wang, J.E. Nevins, Z. Nadler, G. Wollstein, H. Ishikawa, R.A. Bilonick, L. Kagemann, I.A. Sigal, I. Grulkowski, J.J. Liu, M. Kraus, C.D. Lu, J. Hornegger, J.G. Fujimoto, J.S. Schuman, In vivo lamina cribrosa micro-architecture in healthy and glaucomatous eyes as assessed by optical coherence tomography in vivo assessment of 3D LC micro-architecture, *Invest. Ophthalmol. Vis. Sci.* 54 (13) (2013) 8270–8274.
- [38] M.J. Girard, A. Dahlmann-Noor, S. Rayapureddi, J.A. Bechara, B.M.E. Bertin, H. Jones, J. Albon, P.T. Khaw, C.R. Ethier, Quantitative mapping of scleral fiber orientation in normal rat eyes, *Invest. Ophthalmol. Vis. Sci.* 52 (13) (2011) 9684–9693.
- [39] J.K. Pijanka, A. Abass, T. Sorensen, A. Elsheikh, C. Boote, A wide-angle X-ray fibre diffraction method for quantifying collagen orientation across large tissue areas: application to the human eyeball coat, *J. Appl. Crystallogr.* 46 (5) (2013) 1481–1489.
- [40] K.M. Meek, C. Boote, The use of X-ray scattering techniques to quantify the orientation and distribution of collagen in the corneal stroma, *Prog. Retinal Eye Res.* 28 (5) (2009) 369–392.
- [41] J.K. Pijanka, B. Coudrillier, K. Ziegler, T. Sorensen, K.M. Meek, T.D. Nguyen, H.A. Quigley, C. Boote, Quantitative mapping of collagen fiber orientation in non-glaucoma and glaucoma posterior human sclerae, *Invest. Ophthalmol. Vis. Sci.* 53 (9) (2012) 5258–5270.
- [42] B. Baumann, S. Rauscher, M. Glösmann, E. Götzinger, M. Pircher, S. Fialová, M. Gröger, C.K. Hitzemberger, Peripapillary rat sclera investigated in vivo with polarization-sensitive optical coherence tomography, *Invest. Ophthalmol. Vis. Sci.* 55 (11) (2014) 7686–7696.
- [43] C.M. Pierlot, J.M. Lee, R. Amini, M.S. Sacks, S.M. Wells, Pregnancy-induced remodeling of collagen architecture and content in the mitral valve, *Ann. Biomed. Eng.* 42 (10) (2014) 2058–2071.
- [44] U. Tauer, Advantages and risks of multiphoton microscopy in physiology, *Exp. Physiol.* 87 (6) (2002) 709–714.
- [45] H. Tran, N.-J. Jan, D. Hu, A. Voorhees, J.S. Schuman, M.A. Smith, G. Wollstein, I.A. Sigal, Formalin fixation and cryosectioning cause only minimal changes in shape or size of ocular tissues, *Sci. Rep.* 7 (1) (2017) 12065.
- [46] N.-J. Jan, M. Iasella, M. Lester, D. Hu, K.L. Lathrop, A.P. Voorhees, H. Tran, G. Wollstein, J.S. Schuman, I.A. Sigal, Novel method reveals heterogeneous micro-scale response of sclera collagen bundles to homogeneous macro-scale stretch, *Invest. Ophthalmol. Vis. Sci.* 57 (12) (2016). 3566–3566.
- [47] J. Wallace, N.-J. Jan, A. Gogola, M. Iasella, K.L. Lathrop, A.P. Voorhees, H. Tran, I. A. Sigal, Stretch-induced collagen bundle uncrimping and recruitment are independent of depth in equatorial sclera, *Invest. Ophthalmol. Vis. Sci.* 58 (8) (2017). 3162–3162.
- [48] I.A. Sigal, J.L. Grimm, N.-J. Jan, K. Reid, D.S. Minckler, D.J. Brown, Eye-specific IOP-induced displacements and deformations of human lamina cribrosa, *Invest. Ophthalmol. Vis. Sci.* 55 (1) (2014) 1–15.
- [49] H.L. Birch, C.T. Thorpe, A.P. Rumian, Specialisation of extracellular matrix for function in tendons and ligaments, *Muscles Ligaments Tendons J.* 3 (1) (2013) 12–22.
- [50] C.R. Ethier, M. Johnson, J. Ruberti, Ocular biomechanics and biotransport, *Annu. Rev. Biomed. Eng.* 6 (2004) 249–273.
- [51] Z. Nadler, B. Wang, J.S. Schuman, R.D. Ferguson, A. Patel, D.X. Hammer, R.A. Bilonick, H. Ishikawa, L. Kagemann, I.A. Sigal, G. Wollstein, In vivo three-dimensional characterization of the healthy human lamina cribrosa with adaptive optics spectral-domain optical coherence tomography, *Invest. Ophthalmol. Vis. Sci.* 55 (10) (2014) 6459–6466.
- [52] M.J. Girard, J.C. Downs, M. Bottlang, C.F. Burgoyne, J.-K.F. Suh, Peripapillary and posterior scleral mechanics – Part II. Experimental and inverse finite element characterization, *J. Biomech. Eng.* 131 (5) (2009) 051012.
- [53] B. Coudrillier, C. Boote, H.A. Quigley, T.D. Nguyen, Scleral anisotropy and its effects on the mechanical response of the optic nerve head, *Biomech. Model. Mechanobiol.* 12 (5) (2013) 941–963.
- [54] A.P. Voorhees, N.J. Jan, I.A. Sigal, Effects of collagen microstructure and material properties on the deformation of the neural tissues of the lamina cribrosa, *Acta Biomater.* (2017).